Available online at www.sciencedirect.com
SCIENCE DIRECT®
Polymer 44 (2003) 6067–6076
polymer
www.elsevier.com/locate/polymer

Strength and deformation of rigid polymers: the stress–strain curve in amorphous PMMA

Z.H. Stachurski*

Department of Engineering, Faculty of Engineering and Information Technology, Australian National University, Canberra 0200, Australia

Received 20 February 2003; received in revised form 20 May 2003; accepted 2 June 2003

Dedicated to Prof. Ian M. Ward on the occasion of his 75th birthday

Abstract

Poly(methyl methacrylate) (PMMA) is used to model the relaxation and plastic flow mechanisms of deformation, and the characteristic stress–strain response, relating it to its structure as much as it is known. The scope of this work is to identify and quantify the micro-mechanisms and the corresponding stress–strain relationships, and to assemble these into a coherent and self-consistent model for the observed mechanical behaviour. Detailed relationship between relaxation strength and time constants has been derived for some of the secondary motions. It is proposed that plastic events occur when the tension in chain segments pulls the chains out of/through constriction points. The scheme for simulating the isothermal true stress–strain curve is carried out under the following limitations: (i) geometrical effects, such as elastic instability and necking, (ii) thermodynamic adiabatic effects, and (iii) structural and kinetic effects, such as may arise from quenching or annealing, are neglected. Qualitative agreement achieved here is considered satisfactory in view of the simplicity of the model and only a few adjustable parameters.

Keywords: Mechanical model; Anelasticity; Plasticity

1. Introduction

On the most general level, physical mechanisms for plastic deformation can be classified into two main groups:

1. Athermal (dislocation glide, martensite shear transformation, etc.),
2. Thermally activated (dislocation climb, cooperative segmental motions in polymers, grain boundary sliding, etc.).

Physical mechanisms for plastic deformation in polymers have been reviewed [1–7], with the overall conclusion that the phenomena fall into the second category. Thus a complete theory of plasticity for glassy amorphous polymers must involve thermally activated mechanisms. What has always been missing is a direct physical link between the structural elements in the polymer and the observed mechanical behaviour. This relationship has been obscured by lack of a precise, direct method of positioning atoms and description of their displacements. The concise description of plastic flow in metals by a universal relationship involving crystalline structure [8] is far advanced in comparison with the state of plasticity in polymer science, despite similar age of the problem. In the last decade, computer simulations of deformation in polymers have dramatically improved the focus and revealed many features hitherto only hypothesised [9–16]. The basic steps in computer simulations of amorphous polymers include (i) creation of several chains in free space, (ii) subjecting the chains to packing into a cell of target density with periodic boundary conditions, and (iii) a gradual minimisation of the cell potential energy during packing to achieve near-equilibrium structure. Various techniques can be used in the initial stages of packing to ensure randomness of the structure and to equilibrate energy. Velocity scaling is used to control the temperature, so that the probability that a configuration with energy, E, will occur is proportional to the Boltzmann factor. By definition, an equilibrium structure is that in which the force on each atom is zero. The final stage always involves molecular dynamics runs, typically with more than 10^5 steps.

The novel way of representing polymer topology in

* Tel.: +61-2-6125-5681; fax: +61-2-6125-0506.
E-mail address: zbigniew.stachurski@anu.edu.au (Z.H. Stachurski).

0032-3861/03/$ - see front matter © 2003 Elsevier Ltd. All rights reserved.
doi:10.1016/S0032-3861(03)00554-8

terms of Voronoi tessellation based on computer simulations of amorphous polymer cells [17–19] (also described in preceding paper in this volume) provides for a fresh approach to the old problem in the continuing quest to understand plasticity of glassy polymers. Other improvements in techniques, such as NMR [20–22] and positron annihilation spectroscopy [23], combined with careful experimentation, offer corroborating evidence. Taking this information into account, a better understanding of deformation and yield strength can be elucidated in terms of the structural elements characteristic of glassy amorphous polymers. The aim of this work is to identify and quantify the micro-mechanisms and the appropriate stress–strain relationships, and to assemble these into a coherent and self-consistent model for the observed behaviour.

2. Mechanical behaviour

A schematic representation of the stress–strain curve for an amorphous uncrosslinked polymer in its ductile state is shown in Fig. 1. Since the phenomenon of necking is excluded from this description, it is assumed that deformation is homogenous throughout the specimen. The curve is divided along the strain axis into three regions of characteristic behaviour, similarly to the three stages of the stress–strain curve of crystals.

Region I covers the onset of deformation up to the yield point (defined by σ_y, and ε_y). This region is bound on the left by the gradient, $d\sigma/d\varepsilon$ for $\varepsilon \rightarrow 0$, that is the highest possible gradient in the absence of any relaxation processes. At any point, for $\varepsilon > 0$, the actual stress is lower than that because of molecular relaxation effects activated as soon as the sample stress, (σ_s), is greater than zero. This is in accordance with standard stress relaxation experiments and with classical theory of viscoelasticity.

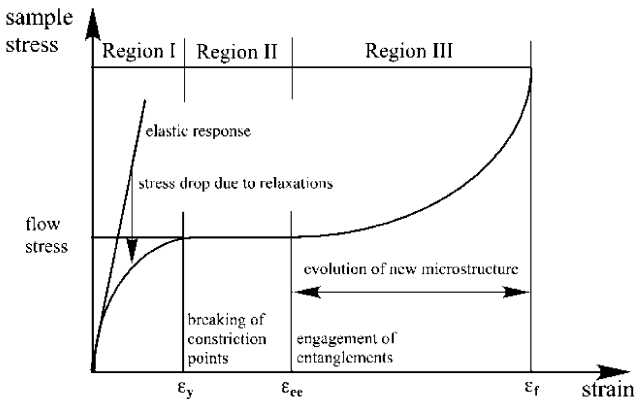

Fig. 1. A schematic representation of the stress–strain curve for amorphous glassy ductile polymer subjected to uniaxial extension at a temperature below its glass transition temperature. Along the horizontal axis are yield strain, entanglement strain and fracture strain. The curve is divided into three regions: (i) anelastic, (ii) plastic flow and (iii) plastic extension with molecular orientation. The division into the three regions of behaviour is described in the text.

The yield point corresponds to the onset of plastic deformation events in the polymer, and is governed by an appropriate yield criterion (on both continuum and atomistic levels). The manifestation of yield is typically at a strain of 0.05 for most glassy polymers [1,2,7]. The process of plastic deformation by the slipping of constriction points is the dominant and self-sustaining process over a significant range of plastic strains [24,25].

Region II is from the onset of yield onwards until the engagement of entanglements strain, ε_{ee} (beyond which further deformation leads to increasing segmental orientation towards the tensile draw direction). Region II is essentially an extension region during which the molecular segments and atomic groups move and deform without significant accumulation of preferred orientation. Homogeneous deformation is assumed. Relaxation motions occur continuously.

Engagement of entanglements between the deforming chains (Region III) leads to the evolution of new nanostructure. The polymer responds to continuing deformation with an increasing drawing stress, mainly due to two effects: (i) increasing value of the elastic modulus with molecular orientation [26], and (ii) increasing value of yield stress due to exhaustion of plastic flow mechanisms, eventually reaching the breaking strength of the oriented polymer, which terminates the third region of behaviour.

2.1. Elastic behaviour

The elastic isotropic modulus can be derived from ab initio calculations, from the principles of molecular mechanics [26–28], or from the fluctuation theorem [29]. The elastic deformations and moduli have been studied extensively, and excellent theoretical formulations exist.

2.2. Anelastic behaviour

Full physical description of anelastic relaxation processes requires two relationships, one for the maximum relative relaxation strength;

$$\left(\frac{\Delta E}{E_U}\right)_\zeta = c_\zeta f_\zeta(\text{molecular parameters and temperature}) \quad (1)$$

and another for the relaxation times;

$$(\tau_R)_i = (\tau_0)_i g_\zeta(\text{molecular parameters and temperature}) \quad (2)$$

where E_U is the unrelaxed value of the modulus, c_ζ is the concentration of the ζ-relaxation mechanism, and f_ζ and g_ζ are functions relating the geometry and dynamics of molecular motions to the structure of the polymer. Given relationships (1) and (2), the stress relaxation modulus can be predicted using the generic form [2]:

$$E_{relax}(t, T, \Omega) = E_U(T, \Omega) - \Delta E(\Omega) H(t, T, \Omega) \quad (3)$$

where E_U is the unrelaxed value of the stress relaxation modulus. The variables inside the brackets indicate func-

tional dependence on time t, temperature T, and structure Ω. The ultimate goal is to define these functions in explicit and precise forms so that the relaxation strength and corresponding relaxation spectrum can be predicted from the structure of the polymer and its thermal history alone.

An amorphous polymer, which exemplifies the many possible molecular relaxation processes, is PMMA. It is used here to model the mechanisms of deformation and its characteristic stress–strain response, in relation to its structure as much as it is known.

The anelastic mechanisms fall into two categories: (i) those limited to motions of the side-groups on the chain, and (ii) those involving segmental motions of chain segments between constriction points. In PMMA, the side-group motions, named previously as motions 1–4, fall into the first category, and the chain segmental motions 5 and 6, into the second [30]. The constriction points divide each macromolecular chain into relatively short segments; for PMMA approximately nine monomers [31]. It is the relaxations within these segments, involving motions 5 and 6, which are responsible for approximately 60% drop in the stress relaxation modulus at long times, in addition to the ~10% drop due to the 1–4 motions.

2.2.1. Summary of side group motions 1–4 in PMMA

A model of the anelastic behaviour in terms of the so-called rotation–translation (RT) model for side branch motions has been published previously [19,30]. The rotation of a side-group (or its fragment) from site 1 to site 2 involves translation of mass. If there is a net displacement of mass between the two sites then stress relaxation can occur. The RT model defines the way for calculation of the maximum relative relaxation strength for these motions, $\Delta E/E_U$ (for $t \rightarrow \infty$), and the spectrum of relaxation times, in terms of precisely defined molecular parameters obtained by Voronoi tessellation method:

$$\left(\frac{\Delta E}{E_U}\right)_{(1-4)} = c_A \frac{1}{\pi} \frac{\bar{d}}{\bar{\Phi}} \frac{\bar{V}_{NAS}}{\bar{V}_{mon}} \tag{4}$$

$$(\tau_R)_{(1-4)} = \tau_0 \exp\left(\frac{Q_1}{k_B T}\right) \exp\left(\frac{q_2/x}{k_B T}\right) \tag{5}$$

where c_A is the concentration of the relaxing species, $\bar{d}$ is the displacement of a net atomic mass (NAS), $\bar{\Phi}$ is the average Voronoi chain diameter, $\bar{V}_{NAS}$ is the average Voronoi volume of the NAS (volume associated with net mass transferred during rotation), and $\bar{V}_{mon}$ is the average Voronoi monomer volume [30]. In PMMA the model distinguishes four possible motions of the side groups (methyl and methacrylate), hence the subscript (1–4). The activation energy for relaxations is divided into two components: one independent of the hindrance due to neighbouring chains (Q_1), and the other (q_2) directly related to the structure of the polymer through the parameter, $x = (V_{mon} - V_0)$, in which V_0 is the minimum Voronoi volume of a monomer. Since there is a distribution of Voronoi volumes, with a ratio of maximum to minimum volume of approximately a factor of two, therefore, relaxation times will have a broad distribution, directly dependent on the nano-structure of the polymer.

Eqs. (3)–(5), predict the magnitude of stress relaxation and the corresponding relaxation times in well defined and measurable molecular quantities, essentially without adjustable factors. The relatively small cooperative nature of these motions (reorientation involves two sites) has been established by NMR measurements [20].

2.2.2. Chain twisting motion 5 in PMMA

Segments of every chain in the polymer must undergo twisting when the polymer sample is subjected to extension. The twisting encounters elastic resistive force resulting from torsional stiffness of the chain, and from the elastic reaction of the matrix. In statistical thermodynamics terms, there is a finite probability that after a characteristic time, τ_R, a twist relaxation will take place. The corresponding molecular rearrangement will result in stress relaxation of a magnitude calculated as [19]

$$\left(\frac{\Delta E(t)}{E_U}\right)_{(5)} = c_B \frac{\alpha(t)}{\varepsilon_{appl}} \tag{6}$$

where $\alpha(t)$ is the angle of twist, and c_B is the concentration of the relaxing species. It is assumed that time, temperature and nano-structural dependence on the corresponding relaxation spectrum and relaxation constants is in accordance with the Adam–Gibbs theory [32,33]:

$$(\tau_R)_{(5)} = \tau_0 \exp\left(\frac{z^* \Delta F}{T S_c}\right) \tag{7}$$

where ΔF is the conventional free energy barrier, z^* is the number of monomers needed to move cooperatively to achieve the translation/transition, and S_c is the configurational entropy associated with that volume.

2.2.3. Chain segment transverse motion 6 in PMMA

The transverse motion 6 of chains is envisaged to take place in segments pinned between constriction points (CPs) as shown in Fig. 2. The chain segment is lying in the plane of the applied/resolved shear stress with the two CPs aligned perpendicular to the direction of the stress. A sphere of diameter equal to the distance, Λ_{CP}, between the CPs is considered as the sphere of local action (activation volume) [4,12]. Under the influence of the stress, the chain segment will suffer displacement, which will be zero at the CPs and maximum in the centre. At some point during the deformation, the relative displacement, a_i, may reach a distance equal to one chain diameter, with consequent strain energy dissipation at the atomic scale. Such a movement will have required the cooperative motion of neighbouring atomic groups in adjacent chains. The maximum relaxation strength, caused by this type of molecular rearrangement,

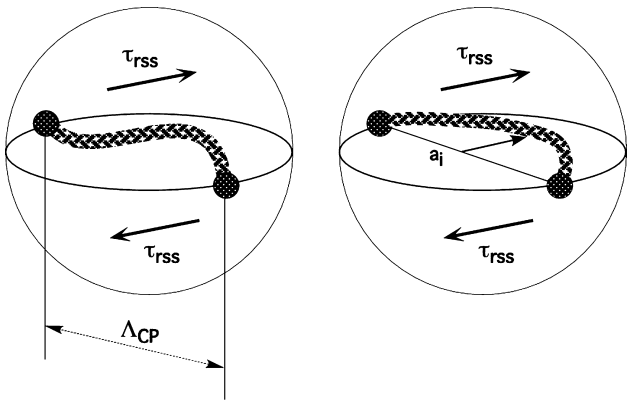

Fig. 2. A schematic drawing of a chain segment subjected to motion 6 mode 1 (transverse to chain axis). The segment is pinned between two constriction points, aligned perpendicular to the direction of the stress. The resolved shear stress causes the segment to displace by a_i. The motion requires cooperative displacements with neighbouring chain segments, maximum at the centre and fading to zero at the boundary of the activation volume (sphere).

can be expressed by the relationship below:

$$\left(\frac{\Delta E}{E_U}\right)_{(6)} = c_C \times \text{geometrical factors} \times \left(\frac{\Delta\varepsilon_{int} \times \text{activation volume}}{\varepsilon_{appl}\Lambda_{CP}^3}\right) \quad (8)$$

where c_C is the concentration of the chain segments, and $\Delta\varepsilon_{int}$ is the 'internal strain' resulting from the molecular rearrangements occurring under the applied strain ε_{appl}. The geometrical factors include (i) $(\pi/6)^{-1}$ from in front of Λ_{CP}^3, and (ii) a function describing the projection of all displacement vectors, a_i (Fig. 2), onto the tensile direction, noting that the magnitude of the displacement is proportional to resolved shear stress, and depends on the angle between the line joining the two CPs and the tensile direction.

Another mode of motion type 6 occurs when the line joining the two CPs is in a plane perpendicular to the plane of maximum resolved shear stress, and perpendicular to the direction of the stress, as shown in Fig. 3. The pinned chain segment is subjected to simple shear deformation with the result of rotation and stretch (or rotation and contraction, depending on the direction of the stress traction). The stretching of the chain segment leads to motion type 5, already described above in Eq. (6).

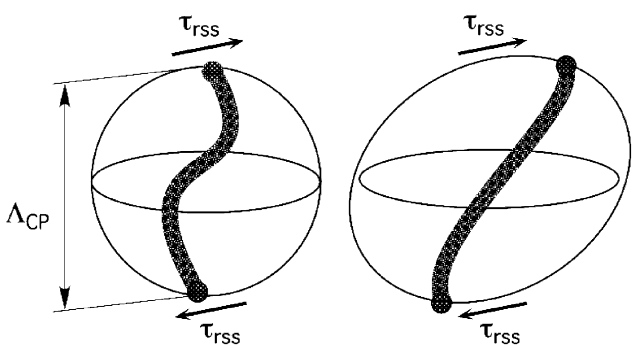

Fig. 3. A schematic drawing of a chain segment subjected to motion 6 mode 2. The resolved shear stress causes the segment to elongate (and rotate). The segment is pinned between two constriction points. The motion requires cooperative displacements with neighbouring chain segments, as in Fig. 2.

The relaxation times for cooperative re-arrangement for motions 5 and 6 are assumed to be given by the Adam and Gibbs theory as in Eq. (7). The time, temperature and nano-structural dependence of the corresponding relaxation spectrum is similar to Eqs. (2) and (7) above.

3. Permanent deformation

3.1. Axial chain motion 7

Both modes (and variations) of motion type 6, described above, lead to stretching of chain segments between CPs. The resulting increasing tension in the chain segments eventually leads to slipping (motion type 7) in the CPs. Plastic events occur when the tension in the chain segment pulls the chain out of/through constriction points [25]. The tensile stress in the sample needed to cause motion 7 is assumed to be given by the following relationship [24]:

$$\sigma_s \geq \sigma_y(T, \Omega) = \beta N_\rho(T)\rho_a(T)f_{max}(\Omega) \quad (9)$$

In the above equation, β is a constant characteristic of a given polymer, $N_\rho(T)$ is equal to the average number of CPs per unit volume, $\rho_a(T)$ is the amorphous density of the polymer, and f_{max} is the maximum force per CP resisting the slipping of the segment (the strength of the constriction point), and Ω indicates dependence on structure.

The dependence of motion 7 on temperature is through the two quantities, $N_\rho(T)$, and $\rho_a(T)$. Whereas the latter is well known (coefficient of thermal expansion $= 2.7 \times 10^{-4}$/K), the variation of the former quantity is related to structural changes in the polymer with temperature, and can be explained with the aid of the diagram in Fig. 4. The diagram shows three distributions of Voronoi monomer volume, calculated for different temperatures as indicated in the figure. The distributions have been drawn in accordance with an equation given previously [31], with the following values used: the exponent, $\alpha = 1.72$; for $T = 328$ K, $V_0 = 0.12$ nm^3, $\lambda = 0.18$, for $T = 378$ K (glass transition temperature) $V_0 = 0.124$ nm^3, $\lambda = 0.20$, and for $T = 428$ K, $V_0 = 0.132$ nm^3, $\lambda = 0.26$. The Voronoi volumes increase with temperature by the normal process of thermal expansion, hence the increasing width and positions of the peaks. The height of the peaks decreases in compliance with the requirement that the area under the peak is constant (conservation of volume), therefore, the increasing value of V_0 (as well as the mean) is obtained by thermal expansion calculations. The number of CPs, i.e. $N_\rho(T)$, is taken as the area under each curve calculated over the interval from V_0 up to

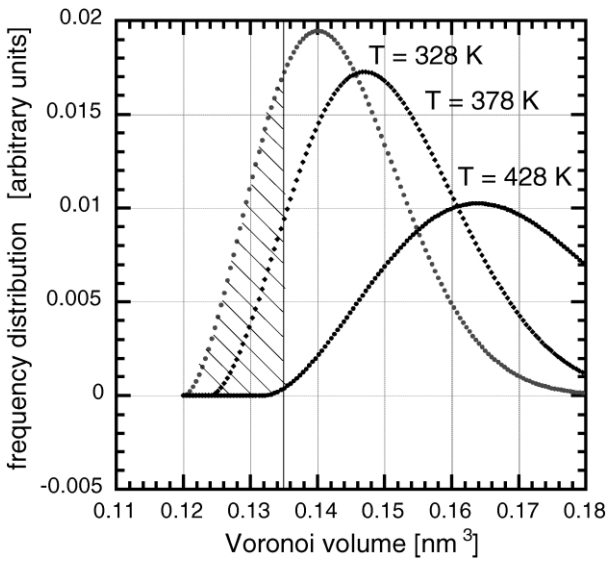

Fig. 4. The distribution of monomer Voronoi volumes at three different temperatures as indicated. The volumes between approximately 0.120 and 0.135 nm^3 (shaded) are considered to be the high density regions containing constriction points. Note that the number of constriction points, represented by the shaded areas, decreases with increasing temperature.

$V_V = 0.135$ nm^3 (it is assumed that the high density regions containing the CPs lie within this interval). Therefore, the three areas indicate the fraction of constriction points expected in the PMMA structure at the three temperatures. The diagram shows that both, the number and strength of the constriction points, decreases markedly with increasing temperature. It is proposed that this is the controlling factor of the experimentally observed falling yield strength (and in general, the effect of transformation into polymer melt).

Yield criterion of the form expressed by Eq. (9) applies typically to athermal processes (glide of dislocations or spontaneous shear). For a thermally activated process the internal plastic flow occurs as soon as the sample is under load, with a strain rate given by [34]

$$\dot{\varepsilon}^{\mathrm{pl}}_{\mathrm{int}} = A \exp\left(-\frac{\Delta F^{\mathrm{pl}} - \sigma_s v_a}{k_B T}\right) \tag{10}$$

where v_a is the activation volume involved in the slip, and ΔF^{pl} is the free energy for plastic flow, comprising two components:

$$\Delta F^{\mathrm{pl}} = F_r + F_s = F_r + (\sigma_y v_a) \tag{11}$$

It is assumed that F_r is the free energy for chain slip in rubbery state, calculated by Edwards and Vilgis [25], and F_s is related to the yield stress given by Eq. (9) and the corresponding activation volume, and it is strongly temperature dependent, decreasing to zero above T_g. The representation of free energy as a sum of two terms is similar to that taken in Eq. (5) above, and it is based on free volume theories of viscoelasticity in polymers [1,2,7]. It follows from Eqs. (10) and (11) that, at temperatures below T_g ($F_r \ll F_s$) and with low values of sample stress, the strain rate is negligibly small. It becomes noticeable when the sample stress, σ_s, approaches σ_y. When $\sigma_s > \sigma_y$, the internal strain rate becomes greater than the applied strain rate, leading to negative slope of the stress–strain relationship.

The magnitude of the incremental stress relaxation due to plastic slip, expressed in terms of the relaxation modulus, is given by

$$\left(\frac{\Delta E}{E_U}\right)^{\mathrm{pl}}_{\Delta t} = N_\rho \frac{\dot{\varepsilon}^{\mathrm{pl}}_{\mathrm{int}}}{\varepsilon_{\mathrm{appl}}} \Delta t \tag{12}$$

3.2. Dilatation and cavitation

The response of an amorphous polymer subjected to hydrostatic tension is dilatation. To a first approximation, the atomic bonding distances increase in proportion to their stiffness, $-\mathrm{d}^2U/\mathrm{d}r^2$, when forced from equilibrium value, r_{eq}. The randomness of chain packing will also cause atomic bonds to bend and twist. The simplest approach, taken here, is to neglect angular bond distortions, and to disregard changes in length of the covalent bonds in view of their relatively high stiffness. What remains to account for is the increase in length of van der Waals bonds, which means effectively a change in inter-chain separation. To a first approximation, the average inter-chain distance in an amorphous polymer can be calculated from [24]

$$\bar{r} \cong \left(\frac{V/l_0}{\pi N}\right)^{1/2} \tag{13}$$

where V is the volume of the polymer, l_0 is the monomer length, and N is the number of monomers in that volume (the exponent of 1/2, sometimes mistakenly given as 1/3, is appropriate to polymers because length changes along the chain axis are miniscule in comparison to transverse variations). To calculate dilatation, the bulk modulus of the polymer must be known. Detailed calculations have been published [15]. It is reasonable to expect that the amount of dilatation will vary from point to point on the nano-scale, due to the density (and hence bulk modulus) fluctuations.

Cavitation is defined here as the physical process of formation of voids under the influence of the applied stress [7,11]. A previous atomistic modelling of cavitation showed it occurring with a sudden stress relief at and above 0.12 dilatational strain [11] (higher than the onset of yielding). Application of multi-axial stress states can be designed to selectively amplify or suppress each process so that the effects can be gauged independently. It is beyond the scope of this paper to treat this matter in any satisfactory detail. However, the point should be made that dilatation will affect all relaxation times (shift to lower times), and the manifestation of cavitation on the stress–strain curve may be very similar to plastic flow. For this reason (and to avoid

masking the yield effect) dilatation and cavitation have not been included in the simulations of the stress–strain curves shown in this paper.

4. Simulation of stress–strain curve

The scheme for simulating the isothermal stress–strain curve is carried out under the following limitations: (i) geometrical effects, such as elastic instability and necking, (ii) thermodynamic adiabatic effects, and (ii) structural and kinetic effects, such as may arise from structural relaxation, are omitted. Finite difference equations method is used to calculate stress and strain increments at each point, which overcomes a requirement for analytical solutions and associated non-linearity of the yield processes. The steps in the simulation process are as follows:

(1) The sample strain is applied stepwise, $\Delta\varepsilon_{\text{appl}}$, at a given strain rate, $\Delta\varepsilon_{\text{appl}}/\Delta t = 0.001/\text{s}$. The sample strain at any time t, after n-steps, is given by

$$\varepsilon_t = \sum_{i=0}^{n} \Delta\varepsilon_i, \qquad t = \Delta t \times n \tag{14}$$

(2) Linear elastic and viscoelastic behaviour is assumed. The corresponding sample stress is calculated by means of the Boltzmann principle of superposition [2]. The elastic stress is diminished at each step by a relaxation function based on relaxation mechanisms defined in terms of molecular motions 1–6, resulting in stress drop [30]:

$$\Delta\sigma_{\text{int}}^{\text{an}} = E_{\text{U}}(\Delta\varepsilon_{\text{appl}} - \Delta\varepsilon_{\text{int}}^{\text{an}}) > 0, \quad \text{condition for viscoelastic solid} \tag{15}$$

where the superscript, 'an', indicates anelastic relaxation.

(3) The isotropic value of the elastic modulus is taken from experimental measurements ($E_0 = 2.3\ \text{GN/m}^2$); its temperature (density) dependence is taken into account [30].

(4) Yield strength, σ_{y}, is calculated from Eq. (9). Its temperature and strain rate dependence is described above.

(5) Incremental stress relaxation by slip occurs with an internal strain rate, $\dot{\varepsilon}_{\text{int}}^{\text{pl}}$ (given by Eq. (10)), which results in internal plastic strain increment,

$$\Delta\varepsilon_{\text{int}}^{\text{pl}} = \dot{\varepsilon}_{\text{int}}^{\text{pl}}\Delta t \tag{16}$$

and the corresponding stress drop:

$$\Delta\sigma_{\text{int}}^{\text{pl}} = E_0(\Delta\varepsilon_{\text{appl}} - \Delta\varepsilon_{\text{int}}^{\text{pl}}) \tag{17}$$

The value of $\Delta\sigma_{\text{int}}^{\text{pl}}$ can be positive or negative, depending on the relative magnitudes of the applied and internal strain increments, similar to the effect described by Brown and Windle [35].

(6) The above process converges, $\sigma_{\text{s}} \rightarrow \sigma_{\text{y}}$. The convergence is monotonic for low applied strain rates and/or high temperatures, or goes through a peak for high strain rates and low temperatures, the effect controlled by strain rate and relaxation times.

(7) Cavitation occurs with an internal strain rate, $\dot{\varepsilon}_{\text{int}}^{\text{cav}}$, which would result in internal plastic strain increment, $\Delta\varepsilon_{\text{int}}^{\text{cav}} = \dot{\varepsilon}_{\text{int}}^{\text{cav}}\Delta t$. The corresponding incremental stress, calculated by finite difference equation, should be

$$\Delta\sigma_{\text{int}}^{\text{cav}} = E_0(\Delta\varepsilon_{\text{appl}} - \Delta\varepsilon_{\text{int}}^{\text{cav}}) \tag{18}$$

In order to be able to distinguish between the plastic flow process and cavitation effects, the latter is not included in the stress–strain calculations shown in Figs. 5 and 6.

(8) The value for the entanglement strain is taken as 0.1. For true strains greater than ε_{ee}, a gradual transformation from isotropic to oriented polymer takes place, leading to the evolution of new nano-structure with new physical and mechanical properties. It is emphasised that the simulation is based on strain, which is assumed to be uniform throughout the specimen. The value of the tensile modulus is made to increase in accordance with the aggregate theory of Ward [26]

$$E(\lambda) = E_0[I_1 + I_2 + 2I_3/(\nu + \nu^2)] \tag{19}$$

where I_1, I_2 and I_3 are orientation parameters which include the draw ratio, $\lambda = 1 + \varepsilon_{\text{appl}}$, and Poisson's ratio, ν.

(9) With stretching, the amount of stress relaxation diminishes in view of the fact that fewer relaxations can take place in a structure composed of oriented chains. As a first approximation, the same Hermans orientation factor [35] is used for all relaxation processes considered here. On further consideration it may be found that individual motions create special local environment in the overall orientation scheme, and different factors may need to be used.

The numerical calculation of yield strength requires

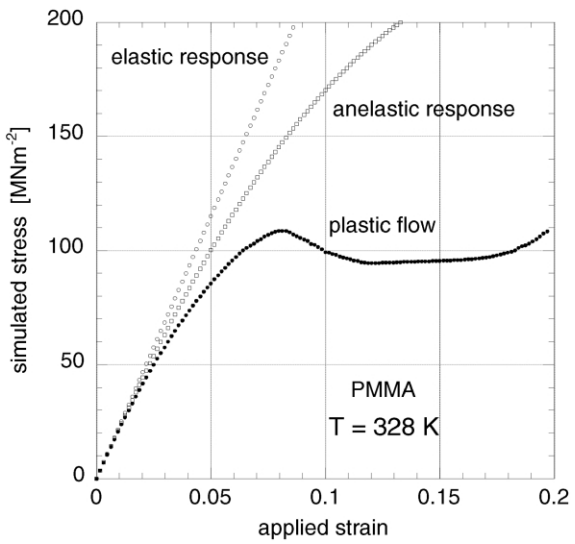

Fig. 5. Simulated stress–strain curve for PMMA subjected to extension at a constant rate of 0.001/s, at $T = 328$ K (50 K below glass transition). At the yield point, the stress drop from elastic to anelastic, and from anelastic to plastic level is approximately the same, showing that plastic flow contributes significantly to stress relaxation.

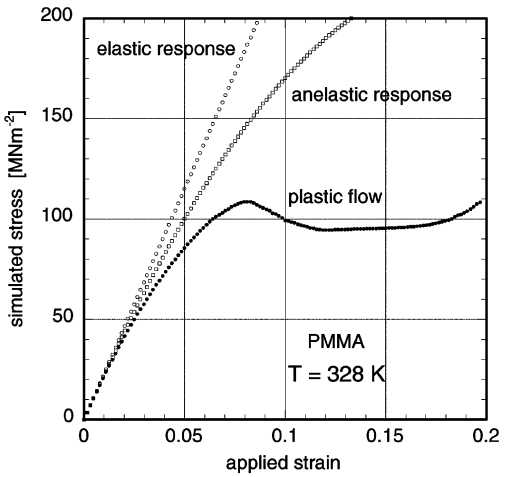

Fig. 6. Simulated stress–strain curve for amorphous glassy PMMA subjected to extension at a constant rate of 0.001/s, at $T = 378$ K (at the glass transition). Note the change in vertical scale from previous graph. No yield point is visible. The stress drop due to plastic flow dominates polymer behaviour.

knowledge of the strength of inter-chain bond, f_{max}. Such a force is a complex function of the many atom-to-atom interactions [18,19]. Its average value can be estimated from cohesive energy density [36], and it is taken as 0.9 nN/monomer (assuming separation of 0.05 nm). The constant, β, includes Schmidt factor, taken approximately as $1/\pi \approx 0.3$, and monomer length over monomer mass, taken as 1.6×10^{15} (m/kg). At $T = 328$ K, density is assumed to be 1120 kg/m^3, and N_ρ, is derived from Fig. 5 as 0.18. Calculation gives the tensile yield strength, $\sigma_y \approx 92$ MN/m^2, higher than the reported values, 60–80 MN/m^2, but considered satisfactory at this stage.

5. Results of stress–strain simulations

Fig. 5 shows three simulated stress–strain curves at $T = 328$ K : a purely elastic response, a viscoelastic response including all motions 1–6, and complete with yield flow. A slight upturn of the curve due to orientation effect at high strains is visible. It can be compared with published stress–strain results for PMMA [37]. The published results show maximum stress at yield for strain approximately 0.08, and stress decreasing after yield up to strain = 0.3; the simulated curve also shows yield point at 0.08, noting the fact that much higher stresses are reached. Fig. 6 shows the corresponding curves for $T = 378$ K. The predicted response at this temperature shows no noticeable yield drop, as expected. The plastic flow levels off sooner, at approximately 0.06, as a result of lower value of the activation energy. Qualitative agreement is considered satisfactory in view of the simplicity of the model and only a few adjustable parameters.

6. Discussion and conclusions

From experimental measurements of plastic behaviour of polymers the following is well established; samples subjected to strains of the order of 5×10^{-2} will recover (given sufficient time). This means there is no permanent set. Consequently, the leading conclusion about the polymer structure is that there is a ‘memory’ network, which allows ‘large’ strains without the structure being destroyed by plastic flow below that strain. The polymer returns to original shape after release of load. The closest analogy is with cross-linked glassy polymers or co-polymers with hard and soft segments. A proposal for such a memory network in uncross-linked polymers has been made previously [38,39]. The concept is based on density fluctuations and the existence of high-density regions. Density fluctuations in polymers have been measured from X-ray scattering [40,41] or indirectly by positron annihilation spectroscopy [23], and for PMMA below T_g the half peak width has been reported as approximately 2%. The corresponding amount derived from Voronoi tessellations is approximately 13% [19]. This is a significant difference, seemingly denying the picture described here for large fluctuations and high density regions on which the concept of CPs depends. However, it is important to recognise that measurements with X-rays probe volumes significantly larger than the average spacing between CPs, which is of the order of $C_K l_0 \sqrt{N_S}$ (~ 1 nm), where N_S is the number of monomers between CPs, l_0 is the monomer length, and C_K is Kuhn constant. Support for the larger value of fluctuations predicted here comes from work on simple systems comprising spheres of equal diameter [42,43], and from computer simulation studies of amorphous polymers [19].

There is a compelling argument from the model presented here, and from previous publication [24], that the mechanism of plastic flow is the slip of chains from the constriction points. This mechanism can only be operative when sufficiently large strain is applied (far greater than that required to move a dislocation)—hence the relatively large yield strain. The point has been made in Ref. [25] that, “reptation is a tiny part of the many different degrees of freedom of the polymer, but it is the motion which allows creep and stress relaxation. In the glassy state the slip link points tighten to the extent that slipping is no longer possible. Some of these pinches will open [under stress] permitting an easier stress–strain relationship than that at zero stress.” In another publication [11] it has been conjectured that plastic slip can only occur by conformational rearrangements in chain molecules of a glassy polymer, primarily only by torsional rotations along the chain backbone. Motions 1–6 described here are consistent with conformational rearrangements and rotations. However, the proposition that these are the only motions for plastic slip is not considered correct since torsional rotations would not account for the memory effect observed.

Temperature dependence of yield stress has been

reported in may publications [1,2,7,44,45]. It is shown here to be related primarily to the structure of the polymer. The variation of amorphous density with temperature is well established. However, the main effect comes from the variation of the quantity, N_ρ, with temperature. This leads to the conclusion that the main source of structural information resides in the distribution of Voronoi volumes. So far only a few Voronoi distributions for polymers have appeared in publications [16–19]. These indicate the existence of details in the distribution, which may provide for the fine differences observed between polymers. Differences between polymers have been stressed by Floudas et al. [40]. A related issue is that of the activation energy for plastic flow, linked directly to the value of the yield stress. The conjecture is that yielding of amorphous glassy polymers is analogous to theoretical shearing of a crystal. The theoretical shear strength of a crystal (Frenkel) is related to the cohesive energy density of the solid. In real crystals shear strength is reduced by defects. In amorphous disordered structures there are no defects to lower their strength. The yield strength is their theoretical shear strength. This accounts for the statement made in the introduction that the strength of amorphous polymers is determined by the strength of the network of strong constriction points, which reside in a matrix of lower density and lower strength.

The upturn of the stress–strain curve at higher strains, referred to as 'strain hardening', is the result of increasing preferred molecular orientation; the strength and stiffness of the covalent bonds contributing more to the load carrying capacity. This is a completely different process from strain hardening in metals, where higher strengths are the result of effects preventing the defects from yielding to the applied load. Thus the real strength of crystalline materials is determined by the network of weaknesses residing in a strong matrix (namely the crystal lattice).

The results of simulations provide further important insight into the mechanism of plastic deformation: first, comparing the simulated curves in Figs. 5 and 6 with experimental curves [37], it is clear that the rapidly varying gradient (compared to that of the anelastic responses) must be related to plastic flow, and cannot be explained by anelastic relaxations. The model employed here has all the relaxation mechanisms included, and their effect is not sufficient to bend the curve at the short time of approximately 50 s to reach yield point. Therefore, the conclusion is that plastic flow itself is engaged gradually, beginning in Region I with a spread of relaxation times.

Structural relaxation in glassy polymers is the cause of the evolution of the ageing peak in DSC scans [46,47]. The excess enthalpy in the system decreases activation barriers, and therefore, increases relaxation rates. This effect will be diminishing with time as the motion of the relaxing species allows for changes of the structure towards more equilibrium state. No allowance for this effect has been included in the results presented here.

The physical process of entanglement engagement is envisaged as shown schematically in Fig. 7. Two chain segments, pinned by their respective CPs, and more or less at right angle with respect to each other, move in such a way that they cross and begin to pull on the chains. This has two consequences. First, the pulling on the CPs contributes to extending plastic flow stress to high strains, and second, since the chains cannot disengage, the drawing process will result in rapid orientation of the segments of the chain (starting at the point of contact), in alignment with the draw direction. The conjecture here is that this is the process leading to the evolution of new microstructure in the polymer, in turn leading to uniaxial orientation with consequent changes in elastic modulus, birefringence, and other physical properties that depend on preferred molecular orientation [48,49]. Another consequence of orientation is diminishing amount of anelastic relaxation. Yet another effect may be at play, where the internal friction is stress dependent. The ratcheting motion, analogous to the motion of a turnstile, rotates the methyl group and is responsible for higher friction at low loads. At higher loads friction decreases, possibly due to screening of the interaction potential or to constraining the excitation modes [50].

A model for the deformation of polymers must conform with the kinematics of chain motions and obey the hierarchy of motions: chain segments cannot move through each other, the motion of a monomer at all times is a consequence of interactions with monomers of surrounding chains and its connectivity to adjacent monomers on its chain, and the motion of a side group at all times is a consequence of interaction with monomers of surrounding chains and its connectivity to the monomer chain. These rules are followed in the model described here.

A major problem to be solved, requiring quantitative molecular-based description, is the relationship between molecular structure and relaxation strengths for motions 5–7, in the same way as it has been achieved for motions 1–4. Eqs. (6), (8) and (12) are physically correct, but too general to prescribe the strengths in a unique, unambiguous way because the relationships between the nano-structure and the corresponding internal strains have not been established.

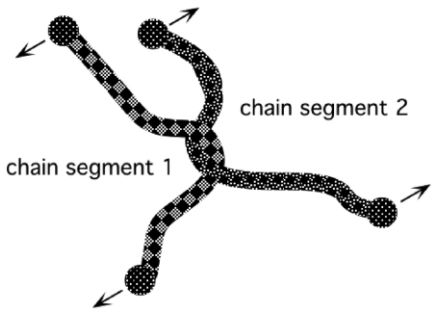

Fig. 7. A schematic drawing of two chain segments crossing each other, and causing an entanglement during plastic deformation. The middle sections of the segments rapidly develop preferred molecular orientation parallel to applied tensile stress.

And yet, these are responsible for a significant part of the mechanical relaxation, amounting to approximately 50–60% of the stress drop. Indeed, for the simulations described here, the strengths were adjusted to give the required modulus drop, without any other justification.

Finally, a model of yield strength cannot distinguish between chain segments on the basis of position along the chain or between the chains, because the number of chains in a volume enveloped by a sphere of diameter equal to the end-to-end distance of a single chain, is proportional to the square root of the number of monomers (very large) in that volume. Therefore, yield strength of amorphous polymers should not depend directly on molecular weight. This is further supported by the assertion that the number of segments per chain is a property of the chain stiffness, and the CPs are expected to partially decouple the dynamics of the chain sections between them, making the relaxation time characteristic of the correlation length of the tight tube, independent of molecular weight. However, molecular weight determines kinetics of cooling (de Gennes chain relaxation times), which determines the nano-structure of the glassy polymer (density, number of CPs per unit volumes, and similar parameters), and therefore, has an indirect effect which is observed experimentally.

There are good reasons to believe that dislocation theories are inappropriate for amorphous polymers. First, the concept of a dislocation as a defect can only be made meaningful when the structure it is to exist in has uniqueness and a sense of order to act as a point of reference. The structure of amorphous polymers cannot be used as a reference to define defects. Second, yield strength of metals decreases with annealing time; the opposite is found in amorphous polymers, as shown in Fig. 8. Third, yield point in metals is observed at strains of the order of 10^{-3} (or less), whereas in polymers it occurs at strains an order of magnitude higher. Fourth, the yield strength in polymers is determined by the strength of a network of constriction points, and not by the defects which exist in crystalline solids.

A number of models dealing with the stress–strain behaviour in polymers have been published, that have the capacity to predict mechanical response to load in terms of microstructural and/or physical parameters related to polymers. The advancement of the present model is in several areas, in particular

1. The deformation of chain segments and side-groups is defined more precisely in terms of the polymer structure using the Voronoi tessellation method, and consequently the magnitude of stress relaxation (and its time, temperature and nano-structure dependence) can be predicted quantitatively. There are fewer ‘adjustable’ parameters used in the theoretical structure of the model, and therefore, the model is more amenable to experimental verification.
2. The physical process of distribution of relaxation times is liked directly to the distribution of Voronoi volumes; in previous methods the distribution of relaxation times was either obtained from experiments, or based on reasonable (but arbitrary) distribution functions.
3. The phenomenon of yield is linked directly to structural features, namely the constriction points. The existence of these has been imagined and proposed well before computer simulations became widely used, and it can be tested experimentally, as has been suggested [31].

Generalisation of the above 1-dimensional model into a 3-dimensional constitutive model is not straightforward. The essential geometrical description of the structure of amorphous solid polymers is not developed yet in sufficient detail (in comparison to the theory of crystallography) to afford the clarity of understanding required to describe precisely individual molecular motions, and the accompanying changes in nano-structure during plastic deformation. The dependence of Poisson’s ratio (or shear modulus) on time, temperature and nano-structure must be established to the same degree of functionality as that described above for the tensile modulus. Only then can the multi-axial constitutive equation be developed in accordance with the general laws of continuum mechanics. Foundation work on the computer simulation of amorphous polymer cells in the

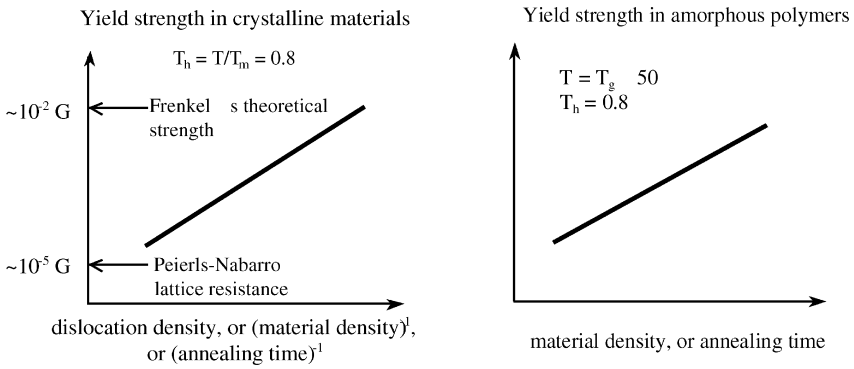

Fig. 8. A comparison of yield strength versus dislocation density or annealing time for pure metals and glassy amorphous polymers. The diagrams show that the yield strength of metals increases with the inverse of annealing time whereas the yield strength of polymers increases in proportion to annealing time.

mid-1980s by Theodorou and Suter, together with the Voronoi method of tessellation, and corroboration from appropriate experimental techniques, offer what is widely regarded as the best means for advancing the understanding of the physical and mechanical behaviour of amorphous polymers.

References

[1] Ward IM. J Mater Sci 1971;6:1397.
[2] Ward IM. Mechanical behaviour of solid polymers, 2nd ed. London: Wiley; 1983. Also.Ward IM, Hadley DW. An introduction to the mechanical properties of solid polymers. Chichester, New York: Wiley; 1993.
[3] Ward IM. J Mater Sci 1973;8:225.
[4] Duckett RA. Int Metals Rev 1983;28:158.
[5] G'Sell C. In: McQueen HJ, Bailon J-P, Dickson JI, Jonas JJ, Akben MG, editors. Strength of metals and alloys. Proceedings of the Seventh International Conference on the Strength of Metals and Alloys, Montreal, Canada, vol. 3.; 1985. p. 1943.
[6] Stachurski ZH. Prog Polym Sci 1997;22(3):407.
[7] Haward RN, Young RJ, editors. The physics of glassy polymers. London: Chapman & Hall; 1997.
[8] Sevillano JG. In: Cahn RW, Haasen P, Kramer EJ, editors. Flow stress and plastic flow in crystals, materials science and technology, vol. 6. Wienheim: VCH; 1993. p. 1.
[9] Theodorou D, Suter UW. Macromolecules 1986;19:379.
[10] Suter UW. Adv Polym Sci 1994;116:1.
[11] Hutnik M, Argon AS, Suter UW. Macromolecules 1991;24:5970.
[12] Argon AS, Mott PH, Suter UW. Phys Stat Sol 1992;172:193.
[13] Mott PH, Argon AS, Suter UW. J Comput Phys 1992;101:140.
[14] Mott PH, Argon AS, Suter UW. Philos Mag 1993;67:931.
[15] Mott PH, Argon AS, Suter UW. Philos Mag 1993;68:537.
[16] Roe RJ, editor. Computer simulation of polymers. New Jersey: Prentice Hall; 1991.
[17] Burkert U, Allinger NL. Molecular mechanics. ACS Monograph 177, Washington: American Chemical Society; 1982.
[18] Mattice WL, Suter UW. Conformational theory of large molecules. New York: Wiley; 1994.
[19] Pfister LA, Stachurski ZH. Polymer 2002;43:7419.
[20] Schmidt-Rohr K, Kulik AS, Beckham HW, Ohlemacher A, Pawelzik U, Boeffel C, Spiess HW. Macromolecules 1994;27:4733.
[21] Utz M, Tomaselli M, Ernst RR, Suter UW. Macromolecules 1996; 29(8):2909.
[22] Maxwell AS, Ward IM, Laupretre F, Monnerie L. Polymer 1998;39: 6835.
[23] Boyce MC. J Polym Sci 1993;31:185.
[24] Stachurski ZH. J Mater Sci 1986;21:3231.
[25] Edwards SF, Vilgis Th. Polymer 1987;28:375.
[26] Ward IM. Proc Phys Soc 1962;80:1176.
[27] Weiner JH. Statistical methods in elasticity. New York: Wiley; 1983.
[28] Theodorou D, Suter UW. Macromolecules 1986;21:3237.
[29] Gusev AA, Zehnder MM, Suter UW. Phys Rev B: Condens Matter 1996;54(1):1.
[30] Stachurski ZH. Polymer 2002;43:7409.
[31] Stachurski ZH. Polymer 2003;44:doi:10-1016/S0032-(03)00555-X.
[32] Adam G, Gibbs JH. J Chem Phys 1965;43:139.
[33] Gómez Ribelles JL, Garayo AV, Cowie JMG, Ferguson R, Harris S, McEwen IJ. Polymer 1998;183.
[34] Duckett RA, Rabonovitz S, Ward IM. J Mater Sci 1970;5:909.
[35] Brown DJ, Windle AH. J Mater Sci 1984;19:2039.
[36] Mathot VBF. Polymer 1984;25:579.
[37] Hasan OA, Boyce MC, Li XS, Berko S. J Polym Sci: Polym Phys 1993;31:185.
[38] Haward RN, Thackray G. Proc R Soc Lond 1968;A302:453.
[39] Boyce MC, Haward RN. In: Haward RN, Young RJ, editors. The physics of glassy polymers. London: Chapman & Hall; 1997.
[40] Floudas G, Pakula T, Stamm M, Fischer EW. Macromolecules 1993; 26:1671.
[41] Rathje J, Ruland W. Colloid Polym Sci 1976;254:358.
[42] Finney JL. Proc R Soc 1970;A319:495.
[43] Reiss H, Hammerich AD. J Chem Phys 1986;90:6252.
[44] Chow TS. Advances in Polym Sci 1992;103:149.
[45] Bicerano J. J Polym Sci: Polym Phys 1991;29:1345.
[46] Estellés JM, Gómez Ribelles JL, Pradas MM. Polymer 1993;34:3837.
[47] Mijovic J, Ho T. Polymer 1993;34:3865.
[48] Ward IM, editor. Structure and properties of oriented polymers. London: Chapman & Hall; 1997.
[49] Haymans N. Polymer 1987;28:2009.
[50] Singer IL. J Vac Sci Technol 1994;A12(5):2605.